Instructions

- Put all files in the same directory.
- Create a folder “resultados” inside this directory.
- Create folders “resultados/resultados#” to save results from different runs. For example, “resultados/resultados1”.
- The w-trick notebook reads eNRG results and averages them. The final, averaged results will be saved in folders “resultados/resultados#/final”. You must create this folder “final”.
- Choose the SIAM parameters for each run in “initial_parameters.txt”. There are four entries: U, V, Vg and w. This last entry is the on site potential of the site coupled to the impurity.
- At the very end of the conductance files, you will find

```
N= 46
folder = 1
dynamical_proprieties(N, folder)
```

This is where you change the “resultados#” folder, and choose the number N of eNRG iterations.

- When this is all done, you can run the conductance files as a normal python script. The two files correspond to the two different eNRG offsets 0 and 1.

the eNRG temperature window can be changed in the function `dynamical_proprieties`, of the conductance files. The UV cut can be changed in `eig_blocks`, of the NRG files.

3.4 Numerical implementation

This section aims to guide our eNRG python code, available at Github*. Readers interested in using our code or learning about the eNRG implementation will benefit from this section. It is not vital for comprehending the rest of this thesis.

The first step in solving a problem requiring the diagonalization of a Hamiltonian is exploring its symmetries. Three conserved quantities of the Anderson Hamiltonian will aid our implementation: particle number and spin,and the spin projection S_z. Consequently, for any NRG iteration, our Hamiltonians will be divided into block-diagonal subspaces of the same charge (Q) and spin (S). Inside each subspace, states with different values of S_z are degenerate. Thus, we only need to take into account one value of s_z, and for simplicity, we take the maximum one. Moreover, a standard definition in the NRG literature is to define half-filling as $Q = 0$.

Let us look at the Hamiltonian (SIAM) of the first eNRG iteration to exemplify these concepts. The shortest possible Wilson chain contains two sites: the impurity and one bath site. The state with a maximum charge has four electrons, the state with a minimum charge has none, and the half-filled state has two electrons. Thus, Q ranges from $-2 \leq Q \leq 2$.

Our basis states also have to be eigenstates of the spin operator. We have no spin when we have no electrons, so $(Q = -2, S = 0)$ is the first subspace we find. By adding one electron, the only possibility for the spin is $S = 1/2$, so the next viable subspace is $(Q = -1, S = 1/2)$. When two states with $S = 1/2$ are added, there are only two possibilities for the spin, i. e. $S = 0$ and $S = 1$. Hence, the half-filled subspaces are $(Q = 0, S = 0)$ and $(Q = 0, S = 1)$. Following the same procedure for all states, we discover all possible subspaces for the first eNRG iteration and notice they have the checker-board structure in Fig. 6. In the implementation, it is crucial to easily identify the labels of a subspace. We achieve this effortlessly if we pay attention to the ordering of the Hamiltonian blocks, which are the arrows in the figure, and this ordering scheme is denoted by diagonal ordering.

The Hamiltonian H_0 and its basis are shown in Eq. 3.49 and Tab. 1 respectively. As aforementioned, because the Hamiltonian has rotational invariance, we only need to perform the diagonalization for states with maximum s_z. For this reason, our initial basis is restricted to just 10 states.

* https://github.com/anarfferrari/Python-eNRG-code

Table 1 – Primitive basis for constructing the first iteration Hamiltonian H_0. Notice how all states have the maximum value of s_z given their spin subspace.

Subspace (Q, S)	Basis $N = 0$
$(2, 0)$	$d^\dagger_\uparrow d^\dagger_\downarrow f^\dagger_{0,\uparrow} f^\dagger_{0,\downarrow} \lvert\emptyset\rangle$
$(1, 1/2)$	$d^\dagger_\uparrow f^\dagger_{0,\uparrow} f^\dagger_{0,\downarrow} \lvert\emptyset\rangle$, $d^\dagger_\uparrow d^\dagger_\downarrow f^\dagger_{0,\uparrow} \lvert\emptyset\rangle$
$(0, 0)$	$\frac{1}{2}\left(d^\dagger_\uparrow f_{0,\downarrow} - d^\dagger_\downarrow f_{0,\uparrow}\right) \lvert\emptyset\rangle$, $d^\dagger_\uparrow d^\dagger_\downarrow \lvert\emptyset\rangle$, $f^\dagger_{0,\uparrow} f^\dagger_{0,\downarrow} \lvert\emptyset\rangle$
$(0, 1)$	$d^\dagger_\uparrow f^\dagger_{0,\uparrow} \lvert\emptyset\rangle$
$(-1, 1/2)$	$d^\dagger_\uparrow \lvert\emptyset\rangle$, $f^\dagger_{0,\uparrow} \lvert\emptyset\rangle$
$(-2, 0)$	$\lvert\emptyset\rangle$

$$H_0 = \begin{pmatrix} 0 & & & & & & & & \\ & V_g & V & & & & & & \\ & V & 0 & & & & & & \\ & & & V_g & & & & & \\ & & & & 2V_g + U & -\sqrt{2}V & 0 & & \\ & & & & -\sqrt{2}V & V_g & -\sqrt{2}V & & \\ & & & & 0 & -\sqrt{2}V & 0 & & \\ & & & & & & & 2V_g + U & -V \\ & & & & & & & -V & V_g \\ & & & & & & & & & 2V_g + U \end{pmatrix} \tag{3.49}$$

After constructing and diagonalizing the Hamiltonian of the first iteration, we must add the following site and build the next Hamiltonian. The small matrix H_0 was computed by hand; however, we need to automate this process. We begin by constructing the new basis by adding a site to the previous basis of eigenstates, i.e. to the *eigenbasis*. Let us say we know the eigenvalues and eigenvectors $E^{Q,S,\ell}_{N-1}$ and $\lvert Q, S, S_z, \ell\rangle_{N-1}$, where ℓ differentiates states inside a subspace, and we bring back the index S_z for the following discussion.

Notice that by adding one site in the Wilson chain, we redefine half-filling, and hence, Q. For example, $\lvert\uparrow,\uparrow\rangle$ is half-filled, but it is one electron short of half-filling in $\lvert\uparrow,\uparrow,\cdot\rangle$. If we add an empty site, the state does not change, but the labels do. Hence, the

Figure 6 – Checker-board structure of the subspaces of $N = 0$, and definition of diagonal ordering.

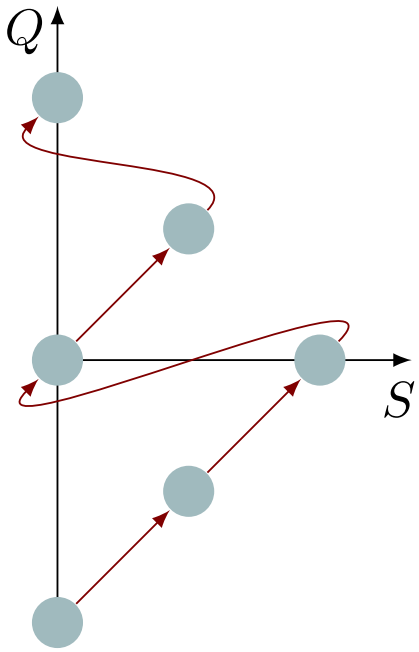

first type of new basis state is

$$|Q-1, S, S_z, p_1\rangle_N^{\mathcal{S}} = \mathcal{O}_S \, |Q, S, S_z, \ell\rangle_{N-1} \tag{3.50}$$

The corresponding operator is labeled $\mathcal{S}$ because the new state belongs to a subspace to the *south* of the one that generates it: its *parent subspace*. Fig 7. aids the understanding of this assertion. By applying the south operator to a state belonging to the subspace in blue of iteration $N-1$, we generate states on the subspace directly below it, in red, of iteration N. Furthermore, notice that we restrict the label ℓ (Eq. 3.50) to the eigenstates and the label p_i to the new state, which is not an eigenstate. The states denoted by p_i for the *primitive basis*. Similarly, we can add a site f_N with two electrons, and we obtain states with the north operator

$$|Q+1, S, S_z, p_2\rangle_N^{\mathcal{N}} = \mathcal{O}_N \, |Q, S, S_z, \ell\rangle_{N-1} \, . \tag{3.51}$$

Adding a site with one electron is slightly trickier as the resulting state must be an eigenstate of the spin operator. Beginning with the subspace (Q, S), the new state must be in the subspace $(Q, S \pm 1/2)$. We have the liberty of choosing any value of S_z that seems fit due to symmetry, and we select

$$|Q, S-\frac{1}{2}, S_z-\frac{1}{2}, p_2\rangle_N^{\mathcal{W}} = O_{\mathcal{W}} \, |Q, S, S_z, \ell\rangle_{N-1} \, , \tag{3.52}$$

and

$$|Q, S+\frac{1}{2}, S_z+\frac{1}{2}, p_3\rangle_N^{\mathcal{E}} = O_{\mathcal{E}} \, |Q, S, S_z, \ell\rangle_{N-1} \, , \tag{3.53}$$

Table 2 – Useful definitions for the eNRG code.

Eigenbasis	Eigenstate of an iteration, labeled by the index ℓ. By operating $\mathcal{O}_\mathcal{N}, \mathcal{O}_\mathcal{S}, \mathcal{O}_\mathcal{E}, \mathcal{O}_\mathcal{W}$ on it, we generate a primitive state. Its elements are called parent states.
Primitive basis	States labeled by p, which form the basis prediagonalization in a certain iteration. Each primitive state has its own gender label, indicating its parent subspace.
Genders	Attribute of the primitive basis, indicating which parent state of the previous iteration generated it.
Invariants	Wigner-Seitz invariants of the parent states, required to construct off-diagonal matrix elements.

In concrete terms, the new states and operators are defined by

$$\mathcal{O}_\mathcal{S} \left|Q, S, S_z, \ell\right\rangle_{N-1} \equiv \left|Q, S, S_z, \ell\right\rangle_{N-1}, \tag{3.54}$$

$$\mathcal{O}_\mathcal{N} \left|Q, S, S_z, \ell\right\rangle_{N-1} \equiv f^\dagger_{N\uparrow} f^\dagger_{N\downarrow} \left|Q, S, S_z, \ell\right\rangle_{N-1}, \tag{3.55}$$

$$\begin{aligned} \mathcal{O}_\mathcal{W} \left|Q, S, S_z, \ell\right\rangle_{N-1} \equiv & \left(\begin{array}{c|cc} S-\frac{1}{2} & \frac{1}{2} & S \\ S_z-\frac{1}{2} & \frac{1}{2} & S_z-1 \end{array}\right) f^\dagger_{N\uparrow} \left|Q, S, S_z-1, \ell\right\rangle_{N-1} \\ & + \left(\begin{array}{c|cc} S-\frac{1}{2} & \frac{1}{2} & S \\ S_z-\frac{1}{2} & -\frac{1}{2} & S_z \end{array}\right) f^\dagger_{N\uparrow} \left|Q, S, S_z, \ell\right\rangle_{N-1}, \end{aligned} \tag{3.56}$$

and

$$\begin{aligned} \mathcal{O}_\mathcal{E} \left|Q, S, S_z, \ell\right\rangle_{N-1} \equiv & \left(\begin{array}{c|cc} S+\frac{1}{2} & \frac{1}{2} & S \\ S_z+\frac{1}{2} & \frac{1}{2} & S_z \end{array}\right) f^\dagger_{N\downarrow} \left|Q, S, S_z, \ell\right\rangle_{N-1} \\ & + \left(\begin{array}{c|cc} S+\frac{1}{2} & \frac{1}{2} & S \\ S_z+\frac{1}{2} & -\frac{1}{2} & S_z+1 \end{array}\right) f^\dagger_{N\uparrow} \left|Q, S, S_z+1, \ell\right\rangle_{N-1}, \end{aligned} \tag{3.57}$$

where the matrices above denote the Clebsch-Gordan coefficients where spins (upper row) and spin projections (lower row) of the right-hand side combine to form the left-hand side.

We say that the eigenstate $\left|Q, S, S_z, \ell\right\rangle_{N-1}$ is the parent of four new basis states, with genders $\mathcal{N}, \mathcal{S}, \mathcal{W}, \mathcal{E}$. Fig. 7 shows this construction. Here, we see how one parent

subspace creates child subspaces in the cardinal directions. In general, subspaces in the four directions are created, except for $S = 0$, where there is no possible subspace to the west. By keeping track of the genders, we know where the state came from (its parent). From the figure, it is also clear that the checker-board structure is maintained in further iterations. Therefore, the diagonal ordering is still well defined. Moreover, we see why even and odd iterations are often distinguished in NRG: only even iterations (in my definition of N) have the subspace $(Q = 0, S = 0)$.

Figure 7 – Construction of the new basis in the checker-board representation. If the parent Subspace has n eigenstates, it generates n states of each gender in its neighbor subspaces.

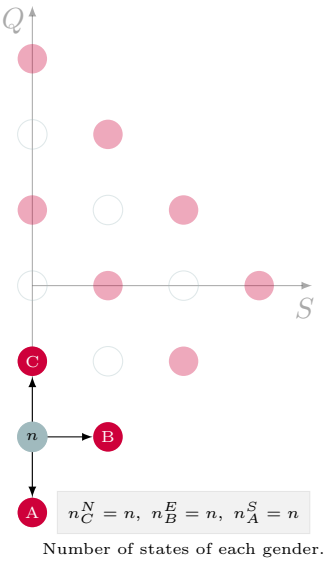

In our code, it is not only the ordering of subspace blocks that matters but also the order of states inside a block. In particular, we order the basis of a specific $H_N^{Q,S}$ by gender $\mathcal{S}$, $\mathcal{W}$, $\mathcal{E}$, and $\mathcal{N}$. This becomes clear once we explain the actual construction of the Hamiltonian matrices.

The Hamiltonian operator, written in terms of a previous iteration, is

$$\mathcal{H}_N = \lambda \mathcal{H}_{N-1} + (f_{N-1}^\dagger f_N + H.c.). \tag{3.58}$$

To compute the diagonal matrix elements, we observe two things. First, the gender operators, which define the new basis, are all unitary and commute with the first term on the left hand side. Therefore,

$$\mathcal{O}_g^\dagger \; H_{N-1} \; \mathcal{O}_g = H_{N-1}. \tag{3.59}$$

Second, the parent states do not contain any operators of site N. Hence, our only chance of having a non-vanishing second term on the left hand side is to combine the operators $\mathcal{O}_g^\dagger$ and $\mathcal{O}_g$ to destroy the site N operator. This is impossible for operators with the same

gender, so that the second term always vanishes. Accordingly, they make no contributions to diagonal matrix elements, and we only need to look at the first term. It does not contain any operators of the added site ($f^\dagger_{N,\sigma}$), and it has exclusively two or four body operators. Therefore, it commutes with the gender operators. Ultimately, the diagonal terms become

$$ {}^{g}\langle q, s, s_z, p|\ \mathcal{H}_N\ |q, s, sz, p\rangle^{g}_{N} = \lambda E^{Q,S,Sz,\ell}_{N-1}, \tag{3.60}$$

where ℓ denotes its parent state. This is why it is essential to know its origin.

To compute the off-diagonal matrix elements, we must work in the same charge and spin subspace (by symmetry) and combine the genders. A general matrix element is

$$\begin{aligned} {}^{g'}\langle q, s, s_z, p'|H^N_A|q, s, s_z, p\rangle^{g}_{N} = \sum_\mu &\langle Q, S, S_z, \ell|\mathcal{O}^\dagger_g(f^\dagger_{N-1\mu}f_{N\mu})\mathcal{O}_{g'}|Q', S', S'_z, \ell'\rangle \\ &+\langle Q, S, S_z, \ell|\mathcal{O}^\dagger_g(f^\dagger_{N\mu}f_{N-1\mu})\mathcal{O}_{g'}|Q', S', S'_z, \ell'\rangle\,. \end{aligned} \tag{3.61}$$

On the left hand side, once again write the primitive basis in terms of its parent states. The off-diagonal operator is a hopping term between site N and $N-1$, while the operators $\mathcal{O}_g$ which generate the primitive basis, only have operators of the site N. This means the gender operators must necessarily differ from one creation/annihilation operator f_N. There can be no extra f_N operator in the matrix element, as they can not be compensated by choice of parent states (which do not contain the site). The first term on the left hand side survives for the gender combinations $\{\mathcal{S},\mathcal{E}\}$, $\{\mathcal{S},\mathcal{W}\}$, $\{\mathcal{W},\mathcal{N}\}$, $\{\mathcal{E},\mathcal{N}\}$. The second term is non vanishing for $\{\mathcal{E},\mathcal{S}\}$, $\{\mathcal{W},\mathcal{S}\}$, $\{\mathcal{N},\mathcal{W}\}$, $\{\mathcal{N},\mathcal{E}\}$. By explicitly writing the gender operators and applying anticommutation relations, we obtain

$$\begin{aligned} {}^{g'}\langle q, s, s_z, p'|H^N_A|q, s, s_z, p\rangle^{g}_{N} = \sum_\mu &\alpha_{g'g}(S, S_z, \mu)\ \langle Q, S, S_z, \ell|f^\dagger_{N-1\mu}|Q', S', S'_z, \ell'\rangle \\ &+\alpha_{gg'}(S, S_z, \mu)\ \langle Q, S, S_z, \ell|f_{N-1\mu}|Q', S', S'_z, \ell'\rangle\,. \end{aligned} \tag{3.62}$$

The $\alpha_{g'g}(S, S_z, \mu)$ coefficients above are known: we can compute them with any gender combination. The most important thing to notice above is that, once again, the matrix element depends on a quantity that comes from the previous iteration. In this case, we the matrix element of parent states. For diagonal terms, we had their energy. Moreover, we can further simplify the equation by using that the Hamiltonian is rotationally invariant so that the Wigner-Seitz theorem applies. We can cast any matrix element as

$$\langle q, s', s'_z|f^\dagger_\mu|q, s, s_z\rangle = \langle q', s'||f^\dagger||q, s\rangle \left(\begin{array}{c|cc} S' & \frac{1}{2} & S \\ S'_z & \mu & S_z, \end{array}\right) \tag{3.63}$$

where the bracket on the left-hand side is an *invariant*. Tab. 3 contains all non zero, non diagonal matrix elements, and Fig. 8 shows the structure of the final Hamiltonian. We order the primitive basis by gender, in $\mathcal{SWEN}$ order. As a consequence, we divide the non-diagonal elements in blocks linking two gender blocks, and we name them *sub-blocks*.

Table 3 – Non zero off diagonal matrix elements of the Nth iteration. Naturally, their conjugates also do not vanish, but they will not be used in our implementation.

g'	g	${}^{g'}\langle q, s, s_z, p'\|H_A^N\|q, s, s_z, p\rangle_N^g$
$\mathcal{E}$	$\mathcal{N}$	$\sqrt{\frac{2s}{2s+1}}\,\langle q, s-1/2, \ell'\|\|f_{N-1}^\dagger\|\|q-1, s, \ell\rangle_{N-1}$
$\mathcal{W}$	$\mathcal{N}$	$-\sqrt{\frac{2s+2}{2s+1}}\,\langle q, s+1/2, \ell'\|\|f_{N-1}^\dagger\|\|q-1, s, \ell\rangle_{N-1}$
$\mathcal{S}$	$\mathcal{E}$	$\langle q+1, s, \ell'\|\|f_{N-1}^\dagger\|\|q, s-1/2, \ell\rangle_{N-1}$
$\mathcal{S}$	$\mathcal{W}$	$\langle q+1, s, \ell'\|\|f_{N-1}^\dagger\|\|q, s+1/2, \ell\rangle_{N-1}$

Figure 8 – Hamiltonian of subpace (Q, S) and iteration N, with its gender quadrants. The colored blocks are the non zero off-diagonal entries, and are called *sub-blocks*. On the left hand side, the central circle in red represents the subspace (Q, S, N), and the circles on the diamond shape are the parent subpaces (of the previous iteration). The sides of the diamond represent the invariants (Tab. 3), which are defined between two parent subspaces. The off-diagonal entries are proportional to them.

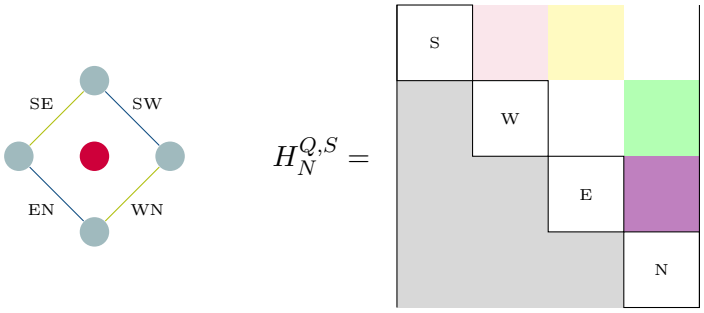

There are critical ingredients for an eNRG/NRG implementation. The first one is the energy of every subspace and iteration. They become the diagonal entries of subsequent iterations. They are also necessary to compute observables, as the many-body energies appear in Boltzmann factors. The next ingredient is the invariants of each iteration, required to compute future off-diagonal elements and matrix elements of interest, i.e., observables. Here, we will discuss how to calculate and store invariants. At last, we also must discuss how to find matrix elements from invariants. We will cover these topics while explaining the code. Functions highlighted in pink are the main fucntions, while the ones in green are auxiliary functions.

Class `Subspace` will be present throughout the code. Each object from this class has three attributes:

- `eigblock`: Index of the parent subspace in the energy array of the previous iteration.

- `invariants`: Array with four entries $(\mathcal{SW}, \mathcal{SE}, \mathcal{EN}, \mathcal{WN})$. Each entry carries the position of the invariants in the invariants array. These are the same labels as Fig. 8.
- `gender`: Array with four entries $(n\mathcal{S}, n\mathcal{W}, n\mathcal{E}, n\mathcal{N})$. Each entry is the number of states with each gender forming the primitive basis.

Iterations will have their own Space matrix, such as in Fig. 9. The entries are the Subspace objects. This construction is useful for quickly accessing and organizing information such as energy and invariant indexes and dimensions of gender blocks (Fig. 8).

Figure 9 – Matriz $N = 0$.

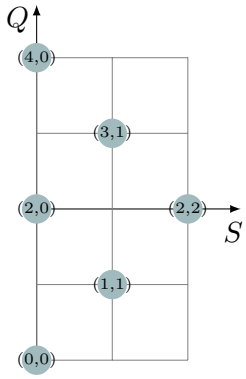

We begin the first iteration $N = 0$ by calling the function `iteration_0`. It defines the initial Hamiltonian Eq. 3.49, diagonalizes it via `eig_blocks`, which implements the *ultra-violet cuttof*. The former function also fills the first space matrix, and the first invariant vector, which we computed analytically.

Fig. 10 shows how we fill the first invariants array and all other iterations will follow the same logic. Because they are matrix elements between parent states of neighboring subspaces, we represent invariants by the diagonal lines. There are two types of invariants: the ones in green pointing to the north-west and the ones in blue pointing to the east-west. The array has size six, corresponding to the six subspaces that can be kets. Following the diagonal ordering, we see the first subspace $(Q = -2, S = 0)$ only has invariants of the green type. Next, $(Q = -1, S = 1/2)$ has invariants of both types. Subspace $(Q = 0, S = 1)$ has invariants of the green and blue kind, but its states are only kets in the blue line. Notice it would be redundant to allocate invariants where states are bras because these matrix elements would already have been allocated as kets of the previous subspace $(Q = -1, S = 1/2)$. Accordingly, the last subspace has an empty entry because it cannot act as a ket.

At the end of iteration zero, we will have the first Space matrix, an array with the many-body energies of all subspaces (below *uv cutoff*), and the invariants array. The next step is calling the function `iteration_N`, which organizes all required steps in

Figure 10 – Structure of the invariant array. It has six entries, for each subspace. The elements are vectors themselves: the first entry carrying invariant of the green kind, and the second entry of the blue kind. Only invariants where the subspace is a ket will be allocated in said subspace.

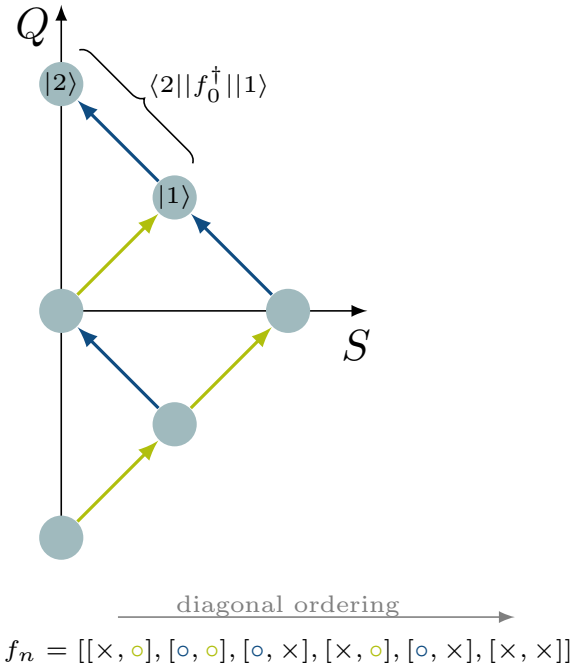

one subroutine. First, we must create the new Space matrix with `new_Space`, which will facilitate the Hamiltonian construction. It generates an empty Space matrix via `empty_Space`, large enough to accommodate the checker-board structure of the current iteration (as in Fig. 9). Function `around_Descendants` fills the subspace objects. It receives a subspace of `Space0` (parent states), with child states in `Space`. The purpose is to keep track of

- the index of the parent energies in the energy array, of the previous iteration;
- the number of child states of each gender subspace (Q, S) creates in the four cardinal directions;
- the position of the relevant invariants in the invariants array.

Fig. 11 expands the explanation on the last item. The subspace in blue belongs to `Space0` and is fed into our function. There is only one entry of the invariants array associated with it: the first one. However, by comparison to Fig. 8, we see that the same invariant enters the sub-block $\mathcal{WN}$ for a state in C and sub-block $\mathcal{SE}$ for a state in B.

With the information provided by `Space` in hands, we construct the new Hamiltonian with function `HN` and organize the basis states by gender in blocks of order

Figure 11 – As shown in Fig. 8, the same invariant contributes to two distinct off-diagonal blocks in the primitive Hamiltonian. For C, the contribution is to the non-diagonal sub-block $\mathcal{WN}$, while for B, the contribution is to $\mathcal{SE}$. The parent subspace does not fill the invariants of the child to south because we are only interested in invariants where the parent state is the ket.

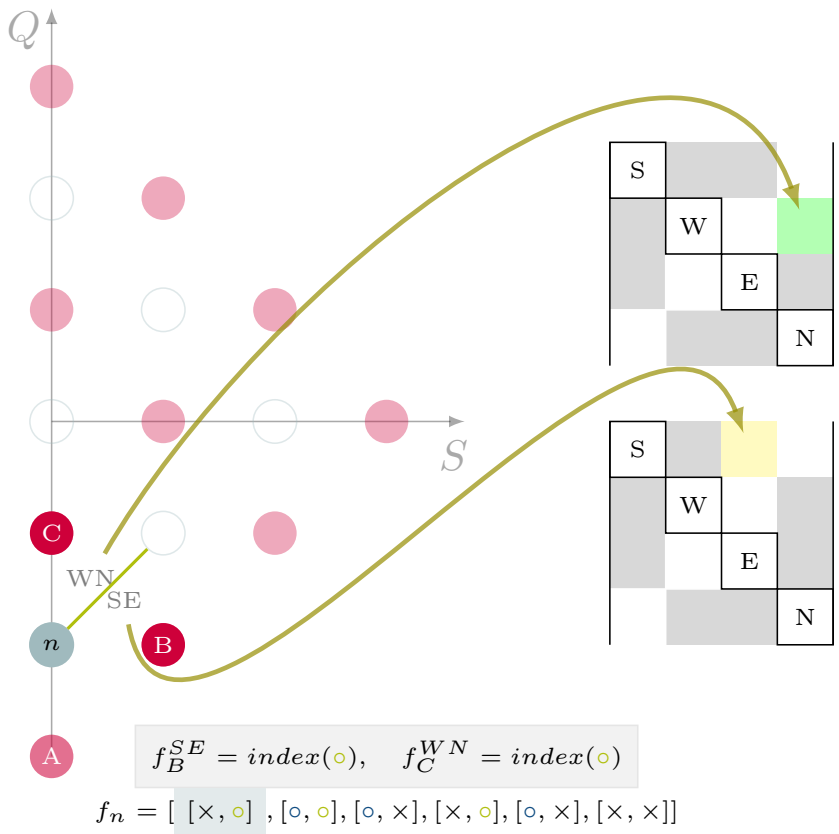

$\mathcal{SWEN}$. The construction of the diagonal part is trivial because the attribute `eigblock` of each subspace is an array with four entries, which are the indexes we need to access the energies of the parents of $\mathcal{SWEN}$. Next, we deal with the off-diagonal part via the function `fills_NonDiagonal`. Here, we know the size of the off-diagonal sub-blocks and the relevant invariants because of the attributes `gender` and `invariants` of `Space`, respectively. The Hamiltonian is then diagonalized by `eig_blocks`, where E_{uv}, the cutoff energy, must be manually changed inside this function.

The last step in every iteration is computing its invariants via `invariants`. We followed the approach detailed in , Sec. *A.4.3. Computation of invariants*. The authors show how to reduce this calculation to multiplications of unitary change of basis matrices (between primitive and parent states) and tabulated coefficients. Despite its simple implementation, this function is the bottleneck of any eNRG/NRG code due to the many matrix multiplications. Although the vital part of our code is in Python language, this specific func-

tion is a Fortran extension to increase performance. Finally, function `matrix_elements` recursively computes the matrix elements of the first bath and impurity sites as they are necessary to find thermoelectric properties. This recursive calculation is the main topic of Pinto et Oliveira [15].

References

1 de Haas, W.; de Boer, J.; van dën Berg, G. The electrical resistance of gold, copper and lead at low temperatures. **Physica**, v. 1, n. 7, p. 1115–1124, 1934. ISSN 0031-8914. Available at: https://www.sciencedirect.com/science/article/pii/S0031891434803102.

2 KONDO, J. Resistance minimum in dilute magnetic alloys. **Progr. Theor. Phys.**, v. 32, n. 1, p. 37–49, 1964.

3 WILSON, K. G. The renormalization group: Critical phenomena and the kondo problem. **Rev. Mod. Phys.**, American Physical Society, v. 47, p. 773–840, Oct 1975.

4 BULLA, R.; COSTI, T. A.; PRUSCHKE, T. Numerical renormalization group method for quantum impurity systems. **Rev. Mod. Phys.**, American Physical Society, v. 80, p. 395–450, Apr 2008. Available at: https://link.aps.org/doi/10.1103/RevModPhys.80.395.

5 PATEL, R.; AGRAWAL, Y.; PAREKH, R. Single-electron transistor: review in perspective of theory, modelling, design and fabrication. **Microsystem Technologies**, Springer, v. 27, n. 5, p. 1863–1875, 2021.

6 BULLA, R. Zero temperature metal-insulator transition in the infinite-dimensional hubbard model. **Phys. Rev. Lett.**, American Physical Society, v. 83, p. 136–139, Jul 1999. Available at: https://link.aps.org/doi/10.1103/PhysRevLett.83.136.

7 MITCHELL, A. K. *et al.* Generalized wilson chain for solving multichannel quantum impurity problems. **Phys. Rev. B**, American Physical Society, v. 89, p. 121105, Mar 2014. Available at: https://link.aps.org/doi/10.1103/PhysRevB.89.121105.

8 STADLER, K. M. *et al.* Interleaved numerical renormalization group as an efficient multiband impurity solver. **Physical Review B**, American Physical Society (APS), v. 93, n. 23, jun 2016. Available at: https://doi.org/10.1103%2Fphysrevb.93.235101.

9 BRUOGNOLO, B. *et al.* Open wilson chains for quantum impurity models: Keeping track of all bath modes. **Phys. Rev. B**, American Physical Society, v. 95, p. 121115, Mar 2017. Available at: https://link.aps.org/doi/10.1103/PhysRevB.95.121115.

10 KRISHNA-MURTHY, H. R.; WILKINS, J. W.; WILSON, K. G. Renormalization-group approach to the anderson model of dilute magnetic alloys. ii. static properties for the asymmetric case. **Phys. Rev. B**, American Physical Society, v. 21, p. 1044–1083, Feb 1980. Available at: https://link.aps.org/doi/10.1103/PhysRevB.21.1044.

11 SILVA, J. B. *et al.* Particle-hole asymmetry in the two-impurity kondo model. **Phys. Rev. Lett.**, American Physical Society, v. 76, p. 275–278, Jan 1996. Available at: https://link.aps.org/doi/10.1103/PhysRevLett.76.275.

12 KRISHNA-MURTHY, H. R.; WILKINS, J. W.; WILSON, K. G. Renormalization-group approach to the anderson model of dilute magnetic alloys. i. static properties for the symmetric case. **Phys. Rev. B**, American Physical Society, v. 21, p. 1003–1043, Feb 1980. Available at: https://link.aps.org/doi/10.1103/PhysRevB.21.1003.

13 YOSHIDA, M.; SERIDONIO, A. C.; OLIVEIRA, L. N. Universal zero-bias conductance for the single-electron transistor. **Physical Review B**, APS, v. 80, n. 23, p. 235317, 2009.

14 BULLA, R. *et al.* Numerical renormalization group for quantum impurities in a bosonic bath. **Phys. Rev. B**, American Physical Society, v. 71, p. 045122, Jan 2005. Available at: https://link.aps.org/doi/10.1103/PhysRevB.71.045122.

15 PINTO, J. W. M.; OLIVEIRA, L. N. Recursive computation of matrix elements in the numerical renormalization group. **Computer Physics Communications**, v. 185, n. 4, p. 1299 – 1309, 2014. ISSN 0010-4655. Available at: http://www.sciencedirect.com/science/article/pii/S0010465514000174.

16 BULLA, R. 12 the numerical renormalization group. **Correlated electrons: from models to materials**.

17 FERRARI, A. L.; OLIVEIRA, L. N. **Real-space numerical renormalization-group computation of transport properties in the side-coupled geometry**. 2021.

18 OLIVEIRA, W. C.; OLIVEIRA, L. N. Generalized numerical renormalization-group method to calculate the thermodynamical properties of impurities in metals. **Physical Review B**, APS, v. 49, n. 17, p. 11986, 1994.

19 OLIVEIRA, W. C.; OLIVEIRA, L. N. Generalized numerical renormalization-group method to calculate the thermodynamical properties of impurities in metals. **Phys. Rev. B**, American Physical Society, v. 49, p. 11986–11994, May 1994. Available at: https://link.aps.org/doi/10.1103/PhysRevB.49.11986.

20 SERIDONIO, A. C.; YOSHIDA, M.; OLIVEIRA, L. N. Universal zero-bias conductance through a quantum wire side-coupled to a quantum dot. **Phys. Rev. B**, v. 80, p. 235318, 2009.

21 YOSHIDA, M.; OLIVEIRA, L. N. d. Thermoelectric effects in quantum dots. **Physica B: Condensed Matter**, Elsevier, v. 404, n. 19, p. 3312–3315, 2009.

22 KIM, T.-S.; HERSHFIELD, S. Thermopower of an aharonov-bohm interferometer: theoretical studies of quantum dots in the kondo regime. **Physical review letters**, APS, v. 88, n. 13, p. 136601, 2002.

23 FROTA, H. O.; OLIVEIRA, L. N. Photoemission spectroscopy for the spin-degenerate anderson model. **Phys. Rev. B**, American Physical Society, v. 33, p. 7871–7874, Jun 1986. Available at: https://link.aps.org/doi/10.1103/PhysRevB.33.7871.

24 LANGRETH, D. C. Friedel sum rule for anderson's model of localized impurity states. **Phys. Rev.**, American Physical Society, v. 150, p. 516–518, Oct 1966. Available at: https://link.aps.org/doi/10.1103/PhysRev.150.516.

25 SCHRIEFFER, J. R.; WOLFF, P. A. Relation between the anderson and kondo hamiltonians. **Phys. Rev.**, American Physical Society, v. 149, n. 2, p. 491–492, 1966.

26 XU, J.-C. *et al.* Ce-site dilution in the ferromagnetic kondo lattice $CeRh_6Ge_4$. **Chinese Physics Letters**, IOP Publishing, v. 38, n. 8, p. 087101, sep 2021. Available at: https://doi.org/10.1088/0256-307x/38/8/087101.

27 KÖHLER, U. **Thermoelectric transport in rare-earth compounds**. December 2007. Tese (Doutorado) — Technical University Dresden, Dresden, Germany, December 2007.